

# Observation of universal dynamics in a spinor Bose gas far from equilibrium

Maximilian Prüfer<sup>1\*</sup>, Philipp Kunkel<sup>1</sup>, Helmut Strobel<sup>1</sup>, Stefan Lannig<sup>1</sup>, Daniel Linnemann<sup>1</sup>, Christian-Marcel Schmied<sup>1</sup>, Jürgen Berges<sup>2</sup>, Thomas Gasenzer<sup>1</sup> & Markus K. Oberthaler<sup>1</sup>

**Predicting the dynamics of quantum systems far from equilibrium represents one of the most challenging problems in theoretical many-body physics<sup>1,2</sup>. While the evolution of a many-body system is in general intractable in all its details, relevant observables can become insensitive to microscopic system parameters and initial conditions. This is the basis of the phenomenon of universality. Far from equilibrium, universality is identified through the scaling of the spatio-temporal evolution of the system, captured by universal exponents and functions. Theoretically, this has been studied in examples as different as the reheating process in inflationary Universe cosmology<sup>3,4</sup>, the dynamics of nuclear collision experiments described by quantum chromodynamics<sup>5,6</sup>, and the post-quench dynamics in dilute quantum gases in non-relativistic quantum field theory<sup>7–11</sup>. However, an experimental demonstration of such scaling evolution in space and time in a quantum many-body system has been lacking. Here we observe the emergence of universal dynamics by evaluating spatially resolved spin correlations in a quasi-one-dimensional spinor Bose–Einstein condensate<sup>12–16</sup>. For long evolution times we extract the scaling properties from the spatial correlations of the spin excitations. From this we find the dynamics to be governed by an emergent conserved quantity and the transport of spin excitations towards low momentum scales. Our results establish an important class of non-stationary systems whose dynamics is encoded in time-independent scaling exponents and functions, signalling the existence of non-thermal fixed points<sup>10,17,18</sup>. We confirm that the non-thermal scaling phenomenon involves no fine-tuning of parameters, by preparing different initial conditions and observing the same scaling behaviour. Our analogue quantum simulation approach provides the basis with which to reveal the underlying mechanisms and characteristics of non-thermal universality classes. One may use this universality to learn, from experiments with ultracold gases, about fundamental aspects of dynamics studied in cosmology and quantum chromodynamics.**

Isolated quantum many-body systems offer particularly clean settings for studying fundamental properties of the underlying unitary time evolution<sup>19</sup>. For systems initialized far from equilibrium, different scenarios have been identified, including the occurrence of many-body oscillations<sup>20</sup> and revivals<sup>21</sup>, the manifestation of many-body localization<sup>22</sup>, and quasi-stationary behaviour in a prethermalized stage of the evolution<sup>23</sup>.

Here we observe a new scenario associated with the notion of non-thermal fixed points. This is illustrated schematically in Fig. 1a: starting from a class of far-from-equilibrium initial conditions, the system develops a universal scaling behaviour in time and space. This is a consequence of the effective loss of details about initial conditions and system parameters long before a quasi-stationary or equilibrium situation may be reached. The transient scaling behaviour is found to be governed by the transport of an emergent collective conserved quantity towards low momentum scales.

For our experimental study we employ an elongated Bose–Einstein condensate of about 70,000 <sup>87</sup>Rb atoms. We use the  $F=1$  hyperfine manifold with its three magnetic sublevels  $m_F=0, \pm 1$  as a spin-1 system with ferromagnetic interactions<sup>24</sup>. Initially, all atoms are prepared in the  $m_F=0$  sublevel, forming a spinor condensate with zero spin length. The dynamics is initiated by instantaneously changing the energy splitting of the  $F=1$  magnetic sublevels by means of microwave dressing (see Methods). Consequently, spin excitations develop in the  $F_x$ – $F_y$  plane<sup>12</sup> as sketched in Fig. 1b. Our experimental setup allows the extraction of the spin distribution in terms of the spin component  $\hat{F}_x(y) = [\hat{\psi}_0^\dagger(y)(\hat{\psi}_{+1}(y) + \hat{\psi}_{-1}(y)) + \text{h.c.}] / \sqrt{2}$  where  $\hat{\psi}_m^\dagger(y)$  is the creation operator of an atom in the magnetic sublevel  $m$  at position  $y$  and h.c. denotes the Hermitian conjugate. At a given time  $t$  this is achieved by a spin rotation from the  $F_x$ – $F_y$  plane to the  $F_z$ -direction and subsequently detecting the atomic density difference  $F_z(y) = n_{+1}(y) - n_{-1}(y)$  (see Methods for details). Representative absorption images are shown in Fig. 1c together with the extracted spin profiles (green lines). The histograms in Fig. 1c show the probability distribution of  $F_x$  for all positions  $y$  and experimental realizations for the corresponding evolution time (see Extended Data Fig. 1 for all evolution times). Results are presented for characteristic stages associated with the initial condition (1), the nonequilibrium instability regime (2), the universal scaling regime (3) and the departure from the non-thermal fixed point (4), as also indicated in Fig. 1a.

We find that during the time evolution the angular orientation  $\theta$  of the transverse spin (see Fig. 1b) becomes the relevant dynamical degree of freedom. For short evolution times unstable longitudinal spin modes grow exponentially<sup>25</sup>, well described by Bogoliubov theory, but non-linear evolution quickly takes over (after about 100 ms). This leads to a double-peaked structure of the histograms (see Fig. 1c) indicating that the spin has a mean length and a random orientation in the  $F_x$ – $F_y$  plane. On the basis of this observation we extract the mean spin length  $\langle |F_\perp(t)| \rangle$ , where  $F_\perp = F_x + iF_y$ , and its fluctuations using a fit. Building on that knowledge, we extract the local angle from the profiles as  $\theta(y, t) = \arcsin(F_x(y, t) / \langle |F_\perp(t)| \rangle)$  (see Methods for details).

The time evolution of the fluctuations of the spin orientation is described in terms of correlation functions of the scalar field  $\theta(y, t)$ . The fluctuations are analysed by evaluating the two-point correlation function  $C(y, y'; t) = \langle \theta(y, t)\theta(y', t) \rangle$ . To distinguish the role of different length scales we consider a momentum-resolved picture of the dynamics. Hence we evaluate the structure factor, which is the Fourier transform of  $C(y, y'; t)$  with respect to the relative coordinate  $\bar{y} = y' - y$ , averaged over  $y$ :

$$f_\theta(k, t) = \int \int dy d\bar{y} C(y + \bar{y}, y; t) \exp(-i2\pi k\bar{y}) \quad (1)$$

In general, the structure factor  $f_\theta$  is a function of momentum  $k$  which evolves in time  $t$  in a way determined by the system parameters and initial conditions. In Fig. 2a, we plot  $f_\theta(k, t)$  as a function of  $k$  on a double-logarithmic scale for times between 4 s and 9 s. A characteristic shift of

<sup>1</sup>Kirchhoff-Institut für Physik, Universität Heidelberg, Heidelberg, Germany. <sup>2</sup>Institut für Theoretische Physik, Universität Heidelberg, Heidelberg, Germany. \*e-mail: universaldynamics@matterwave.de

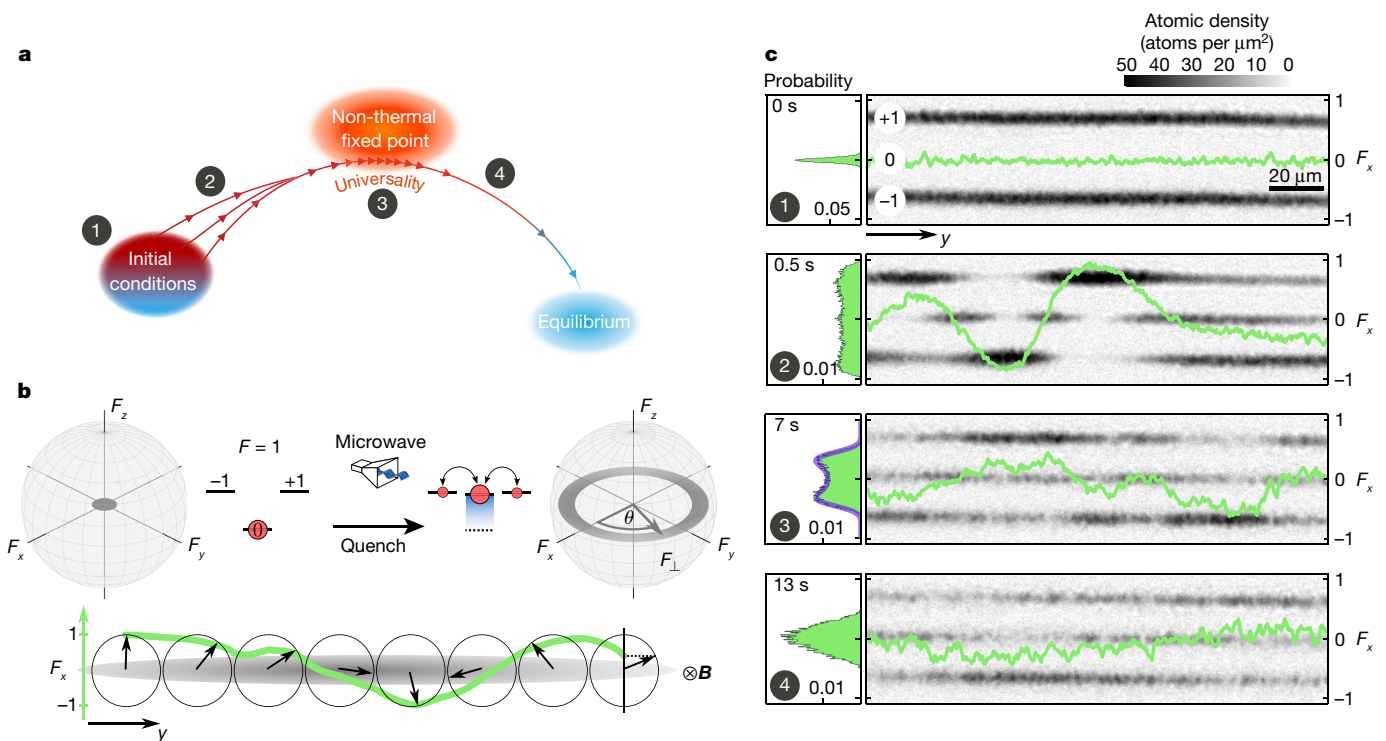


**Fig. 1 | Universal dynamics and experimental procedure.** **a**, Starting from a class of far-from-equilibrium initial conditions, universal dynamical evolution indicates the emergence of a non-thermal fixed point. Experimentally, we probe the system at different evolution times during the stages indicated by numbers 1 to 4. **b**, A condensate is prepared in the  $m_F=0$  state of the  $F=1$  hyperfine manifold, that is, with a vanishing mean spin length (left spin sphere). With microwave dressing (see Methods) we initiate spin-exchange dynamics, which leads to a growth of spin orthogonal to the magnetic field  $\mathbf{B}$  in the  $F_x$ - $F_y$  plane (right spin sphere).

Subsequently, spatial structures of the spin orientation  $\theta$  are found along the cloud. **c**, Exemplary absorption images of the three hyperfine levels taken after a  $\pi/2$  spin rotation and Stern–Gerlach separation together with the inferred local spin  $F_x(y)$  (green lines). Furthermore, histograms for around 160 experimental realizations are shown. In the universal regime (see step 3 in panel **a**) we extract the spin length and its fluctuation by a fit to the double-peaked structure of the histogram, as indicated in the corresponding plot (see Methods).

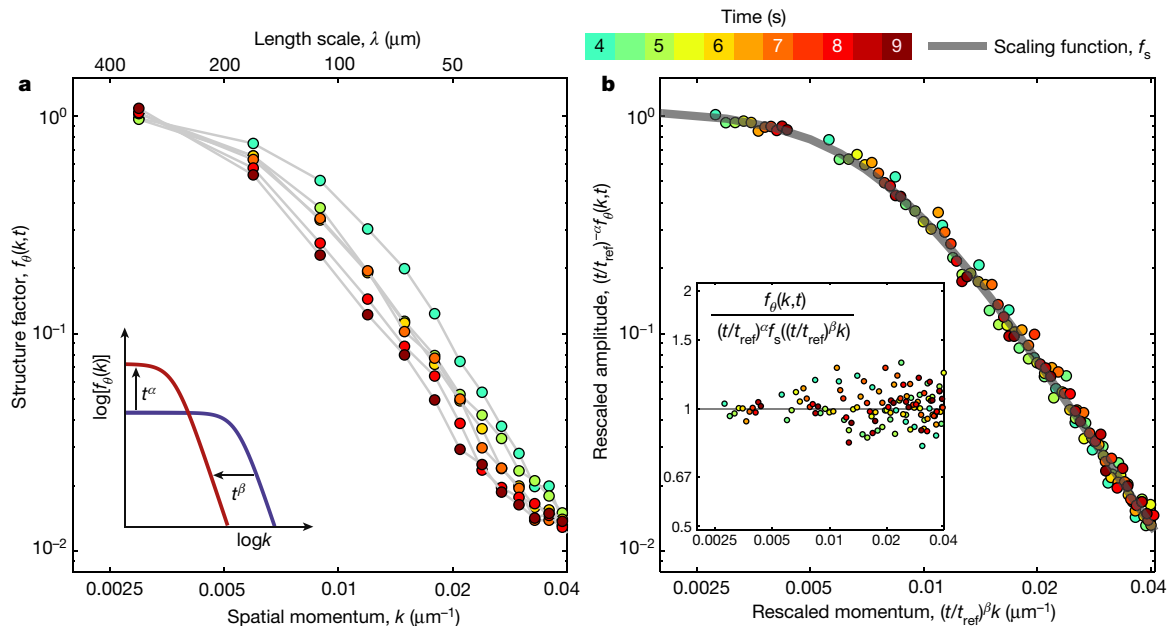


**Fig. 2 | Scaling in space and time at a non-thermal fixed point.** **a**, Structure factor  $f_\theta(k,t)$  as a function of the spatial momentum  $k=1/\lambda$  in the scaling regime between 4 s and 9 s. The colour indicates the evolution time  $t$ . The statistical error is of the order of the size of the plot markers. In the infrared the structure factor shifts in time to smaller  $k$  (bigger wavelengths), which is connected to transport of excitations towards lower momenta. Characteristic for the non-thermal fixed point dynamics is the

rescaling of the amplitude with universal exponent  $\alpha$  and rescaling of the length scale with  $\beta$  (see inset). **b**, By rescaling the data with  $t_{\text{ref}}=4.5$  s,  $\alpha=0.33$  and  $\beta=0.54$  the data collapses to a single curve. We parameterize the universal scaling function with  $f_s \propto 1/[1+(k/k_s)^\zeta]$ . Using a fit (grey solid line) we find  $\zeta \approx 2.6$  and  $k_s \approx 1/133 \mu\text{m}^{-1}$ . The quality of the rescaling is revealed by the small and symmetric scatter of the rescaled data divided by the fit (see inset).

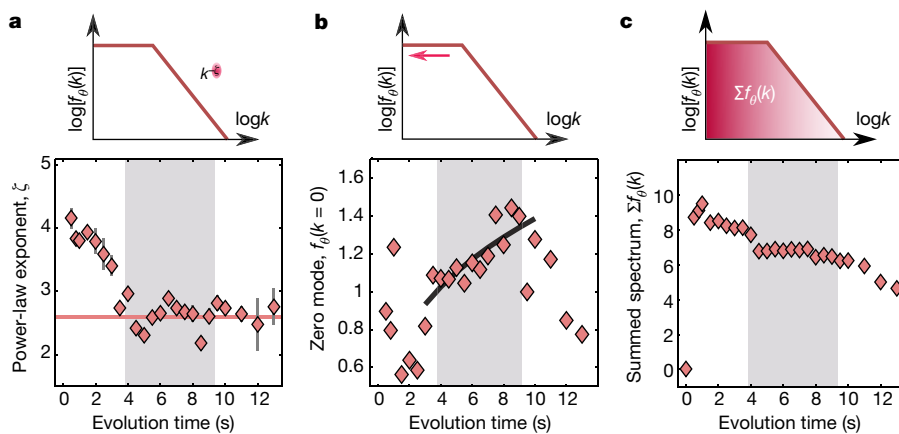


**Fig. 3 | Characterization of the scaling regime.** **a**, For each evolution time (see Fig. 2) we extract the power-law exponent  $\zeta$  from a fit. After 4 s it settles to about 2.6 (red solid line), revealing the build-up of the universal scaling function. The grey-shaded region indicates the scaling regime. **b**, The transport to the infrared in the scaling regime is connected to a monotonic increase of the occupation of  $k = 0$ . The solid line depicts

the expected scaling  $f_0(k=0, t) \propto t^\alpha$  with  $\alpha = 0.33$ . After 9 s a rapid decay signals the departure from the scaling regime. **c**, The emergence of a conserved quantity is signalled by the sum over all  $k$ -modes of  $f_0(k, t)$ . After a fast initial growth this observable is approximately constant in the scaling regime and starts to decay after 9 s.

the structure factor towards smaller momenta as well as an increase of the low-momentum amplitude with time is observed.

In fact, instead of separately depending on  $k$  and  $t$  we find that in this regime the datasets collapse to a single curve if the rescaled distribution  $t^{-\alpha} f_0$  is plotted as a function of the single variable  $t^\beta k$ . This implies that the data satisfy the scaling form

$$f_0(k, t) = t^{\alpha} f_s(t^{\beta} k) \quad (2)$$

with universal scaling exponents  $\alpha, \beta$  and scaling function  $f_s$ . Figure 2b shows this collapse, where the same data points as in Fig. 2a are plotted with times normalized to the reference time  $t_{\text{ref}} = 4.5$  s. The ability to reduce the full nonequilibrium time evolution of the correlation function in the scaling regime to a time-independent, so-called fixed-point distribution  $f_s(k)$  and associated scaling exponents is a striking manifestation of universality.

We find the amplitude scaling exponent to be  $\alpha = 0.33 \pm 0.08$  and the momentum scaling exponent to be  $\beta = 0.54 \pm 0.06$ . The errors correspond to one standard deviation obtained from a resampling technique (see Methods). However, the actual uncertainty for  $\alpha$  is expected to be larger since the rescaling analysis is much less constraining on  $\alpha$  than on  $\beta$ . We find that  $f_0(k, t)$  develops a plateau at the lowest momenta and an approximate power-law fall-off above a characteristic length scale in the scaling regime. To parameterize the universal scaling function, we fitted the rescaled data with a function of the form<sup>26</sup>:  $f_s(k) \propto 1/[1 + (k/k_s)^\zeta]$  and find  $\zeta \approx 2.6$ , with  $k_s \approx 1/133 \mu\text{m}^{-1}$  for our system. The value of  $\zeta$  becomes constant after about 4 s (see Fig. 3a). Analysing  $f_0(k=0, t)$  as shown in Fig. 3b reveals that the occupation of  $k=0$ , which cannot be seen on the logarithmic scale employed in Fig. 2, builds up in the scaling regime. This growth is consistent with the power law proportional to  $t^\alpha$  with  $\alpha$  obtained from the rescaling analysis, as indicated by the solid line. After 9 s the system departs from the scaling behaviour.

The nature of the observed scaling phenomenon is explained by the emergence of an approximately conserved quantity and its transport. In terms of our dynamical degree of freedom  $\theta(y, t)$  we identify  $\int dk \langle |\theta(k, t)|^2 \rangle \equiv \int dk f_0(k, t)$  as the conserved quantity. In fact, Fig. 3c shows that the sum over all modes  $k$  for different evolution times—after a fast initial rise due to the instability—settles around a constant within the scaling regime (see also Extended Data Fig. 2). According to the scaling (2),  $\int dk f_0(k, t) = t^{\alpha-\beta} \int dk f_s(k) \approx \text{const.}$  corresponds to  $\alpha \approx \beta$  so that in our case only one independent dynamical scaling exponent remains. A distinct feature is the transport of the conserved quantity directed towards the infrared, corresponding to a positive sign of  $\beta$ . Theoretically it is expected to find the scaling only for momenta smaller

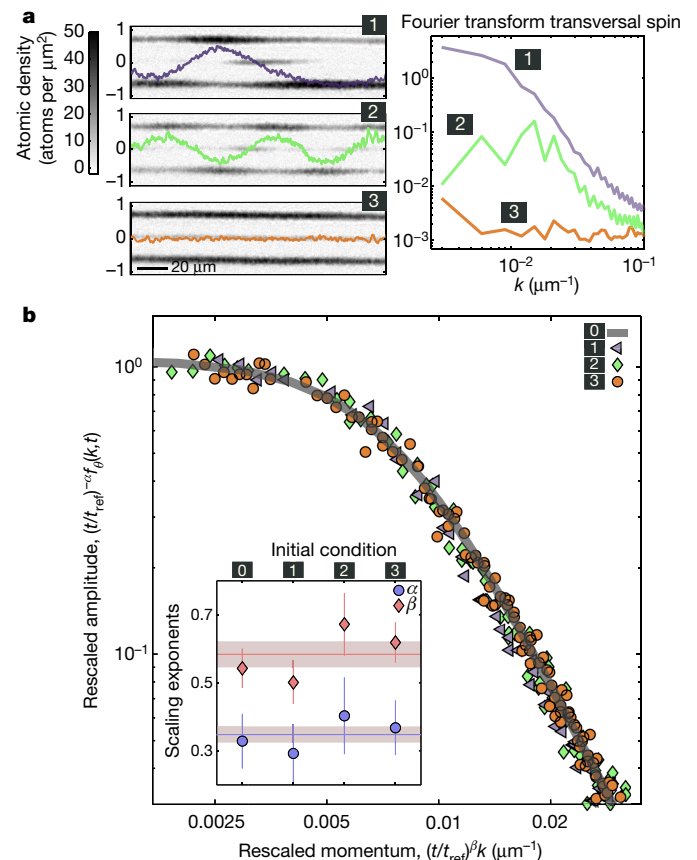


**Fig. 4 | Robustness of universal dynamics at a non-thermal fixed point.**

**a**, Absorption images of all three  $m_F$  components after spin rotation with the extracted transversal spin (solid lines) of three different initial conditions. The preparations show different initial amplitudes in the Fourier transform of the transversal spin. **b**, All initial conditions lead to scaling dynamics. The data shown were obtained in a time window between 4 s and 9 s after preparation of the initial state. In the inset the scaling exponents of all four initial conditions, including the preparation in  $m_F = 0$  (see Fig. 1), are shown; the error bars are 1 s.d., obtained from a resampling method (see Methods). The mean values (red and blue solid lines) of  $\alpha$  and  $\beta$  are used to rescale the data. We allow for overall scaling factors in  $k$  and amplitude for each initial condition.



than some scale<sup>10</sup> (in our case about  $0.04 \mu\text{m}^{-1}$ ; see Extended Data Fig. 3). The transport towards the infrared is in contrast to the turbulent transport into the ultraviolet observed in direct cascades<sup>27</sup>.

These experimental findings of scaling behaviour, implying universality, allow comparison with predictions in a variety of models in the non-thermal universality class, which is defined by the scaling function  $f_s$  and  $\alpha = d\beta$  for given spatial dimension  $d$ .  $N$  interacting Bose gases with equal intra- and interspecies Gross–Pitaevskii couplings are described by an  $O(N)$  symmetric model. This is closely related to  $O(N)$  symmetric scalar models<sup>28</sup>, such as the relativistic Higgs sector of the Standard Model with  $N = 4$  for  $d = 3$ . For these types of models, both Gross–Pitaevskii and relativistic, a universal value of  $\beta \approx 0.5$  has been predicted and found to be insensitive to the spatial dimension<sup>10</sup> for  $d \geq 2$ . This describes the self-similar transport of excitations of the relative phases between the components to lower wavenumbers. The scaling function  $f_s$  is known to depend on dimensionality<sup>29</sup> and has not yet been theoretically estimated for  $d = 1$ . Our setup is, to our knowledge, the first realization of an effective  $N = 3$  model for the transport of conserved quantities associated with non-thermal fixed points in a quasi-one-dimensional situation. Finding scaling behaviour in one dimension was not expected and sheds new light on the concept of universality classes far from equilibrium.

We emphasize that the non-thermal scaling phenomenon studied here involves no fine-tuning of parameters. This is in contrast to equilibrium critical phenomena, which require a careful adjustment of system variables, such as the temperature, to a critical value<sup>30</sup>. To illustrate this insensitivity we employ the high level of control of the atomic spin system and prepare three qualitatively different initial conditions (for details see Methods). The corresponding absorption images of single realizations are shown in Fig. 4a along with the Fourier transform of the spatial correlation function of  $F_s(y)$ .

We find universal dynamics for all initial conditions with comparable inferred scaling exponents (see inset of Fig. 4b). We rescale the data with the same exponents obtained from the mean of all four measurements and take into account overall scaling factors and reference momentum scales. This procedure leads to a collapse of all data, manifesting the robustness of non-thermal fixed point scaling.

The level of control demonstrated here and the accessible observables on our platform open the door to the discovery of further non-thermal universality classes. This represents a crucial step towards a comprehensive understanding of out-of-equilibrium dynamics with potential impact in various fields of science.

(We note that similar phenomena have recently been observed by the Schmiedmayer group<sup>31</sup> in Vienna in a single-component Bose gas, where a scaling exponent  $\beta \approx 0.1$  was extracted.)

## Online content

Any methods, additional references, Nature Research reporting summaries, source data, statements of data availability and associated accession codes are available at <https://doi.org/10.1038/s41586-018-0659-0>.

Received: 29 March; Accepted: 28 September 2018;

Published online 7 November 2018.

1. Polkovnikov, A., Sengupta, K., Silva, A. & Vengalattore, M. Nonequilibrium dynamics of closed interacting quantum systems. *Rev. Mod. Phys.* **83**, 863–883 (2011).
2. Eisert, J., Friesdorf, M. & Gogolin, C. Quantum many-body systems out of equilibrium. *Nat. Phys.* **11**, 124–130 (2015).
3. Kofman, L., Linde, A. & Starobinsky, A. A. Reheating after inflation. *Phys. Rev. Lett.* **73**, 3195–3198 (1994).
4. Micha, R. & Tkachev, I. I. Relativistic turbulence: a long way from preheating to equilibrium. *Phys. Rev. Lett.* **90**, 121301 (2003).
5. Baier, R., Mueller, A. H., Schiff, D. & Son, D. “Bottom-up” thermalization in heavy ion collisions. *Phys. Lett. B* **502**, 51–58 (2001).
6. Berges, J., Boguslavski, K., Schlichting, S. & Venugopalan, R. Turbulent thermalization process in heavy-ion collisions at ultrarelativistic energies. *Phys. Rev. D* **89**, 074011 (2014).
7. Lamacraft, A. Quantum quenches in a spinor condensate. *Phys. Rev. Lett.* **98**, 160404 (2007).

8. Barnett, R., Polkovnikov, A. & Vengalattore, M. Prethermalization in quenched spinor condensates. *Phys. Rev. A* **84**, 023606 (2011).
9. Hofmann, J., Natu, S. S. & Das Sarma, S. Coarsening dynamics of binary Bose condensates. *Phys. Rev. Lett.* **113**, 095702 (2014).
10. Piñeiro Orioli, A., Boguslavski, K. & Berges, J. Universal self-similar dynamics of relativistic and nonrelativistic field theories near nonthermal fixed points. *Phys. Rev. D* **92**, 025041 (2015).
11. Williamson, L. A. & Blakie, P. B. Universal coarsening dynamics of a quenched ferromagnetic spin-1 condensate. *Phys. Rev. Lett.* **116**, 025301 (2016).
12. Sadler, L. E., Higbie, J. M., Leslie, S. R., Vengalattore, M. & Stamper-Kurn, D. M. Spontaneous symmetry breaking in a quenched ferromagnetic spinor Bose–Einstein condensate. *Nature* **443**, 312–315 (2006).
13. Kronjäger, J., Becker, C., Soltan-Panahi, P., Bongs, K. & Sengstock, K. Spontaneous pattern formation in an antiferromagnetic quantum gas. *Phys. Rev. Lett.* **105**, 090402 (2010).
14. Bookjans, E. M., Vinit, A. & Raman, C. Quantum phase transition in an antiferromagnetic spinor Bose–Einstein condensate. *Phys. Rev. Lett.* **107**, 195306 (2011).
15. De, S. et al. Quenched binary Bose–Einstein condensates: spin-domain formation and coarsening. *Phys. Rev. A* **89**, 033631 (2014).
16. Nicklas, E. et al. Observation of scaling in the dynamics of a strongly quenched quantum gas. *Phys. Rev. Lett.* **115**, 245301 (2015).
17. Berges, J., Rothkopf, A. & Schmidt, J. Nonthermal fixed points: effective weak coupling for strongly correlated systems far from equilibrium. *Phys. Rev. Lett.* **101**, 041603 (2008).
18. Nowak, B., Sexty, D. & Gasenzer, T. Superfluid turbulence: nonthermal fixed point in an ultracold Bose gas. *Phys. Rev. B* **84**, 020506(R) (2011).
19. Bloch, I., Dalibard, J. & Nascimbène, S. Quantum simulations with ultracold quantum gases. *Nat. Phys.* **8**, 267–276 (2012).
20. Hung, C.-L., Gurarie, V. & Chin, C. From cosmology to cold atoms: observation of Sakharov oscillations in a quenched atomic superfluid. *Science* **341**, 1213–1215 (2013).
21. Rauer, B. et al. Recurrences in an isolated quantum many-body system. *Science* **360**, 307–310 (2018).
22. Schreiber, M. et al. Observation of many-body localization of interacting fermions in a quasirandom optical lattice. *Science* **349**, 842–845 (2015).
23. Gring, M. et al. Relaxation and prethermalization in an isolated quantum system. *Science* **337**, 1318–1322 (2012).
24. Stamper-Kurn, D. M. & Ueda, M. Spinor Bose gases: symmetries, magnetism, and quantum dynamics. *Rev. Mod. Phys.* **85**, 1191–1244 (2013).
25. Leslie, S. R. et al. Amplification of fluctuations in a spinor Bose–Einstein condensate. *Phys. Rev. A* **79**, 043631 (2009).
26. Karl, M. & Gasenzer, T. Strongly anomalous non-thermal fixed point in a quenched two-dimensional Bose gas. *New J. Phys.* **19**, 093014 (2017).
27. Navon, N., Gaunt, A. L., Smith, R. P. & Hadzibabic, Z. Emergence of a turbulent cascade in a quantum gas. *Nature* **539**, 72–75 (2016).
28. Zinn-Justin, J. *Quantum Field Theory and Critical Phenomena* (Clarendon Press, Oxford, 2002).
29. Chantesana, I., Piñeiro Orioli, A. & Gasenzer, T. Kinetic theory of non-thermal fixed points in a Bose gas. Preprint at <http://arXiv.org/abs/1801.09490> (2018).
30. Hohenberg, P. C. & Halperin, B. I. Theory of dynamic critical phenomena. *Rev. Mod. Phys.* **49**, 435–479 (1977).
31. Erne, S., Bücker, R., Gasenzer, T., Berges, J. & Schmiedmayer, J. Universal dynamics in an isolated one-dimensional Bose gas far from equilibrium. *Nature* <https://doi.org/10.1038/s41586-018-0667-0> (2018).

**Acknowledgements** We thank D. M. Stamper-Kurn, J. Schmiedmayer, A. Piñeiro Orioli, M. Karl, J. M. Pawłowski and A. N. Mikheev for discussions. This work was supported by the Heidelberg Center for Quantum Dynamics, the European Commission FET-Proactive grant AQuS (project number 640800), the ERC Advanced Grant Horizon 2020 EntangleGen (project ID 694561) and the DFG Collaborative Research Center SFB1225 (ISOQUANT).

**Reviewer information** Nature thanks M. Kolodrubetz and the other anonymous reviewer(s) for their contribution to the peer review of this work.

**Author contributions** The experimental concept was developed in discussion among all authors. M.P., P.K. and S.L. controlled the experimental apparatus. M.P., P.K., H.S., S.L. and M.K.O. discussed the measurement results and analysed the data. C.-M.S., J.B. and T.G. elaborated the theoretical framework. All authors contributed to the discussion of the results and the writing of the manuscript.

**Competing interests** The authors declare no competing interests.

## Additional information

**Extended data** is available for this paper at <https://doi.org/10.1038/s41586-018-0659-0>.

**Reprints and permissions information** is available at <http://www.nature.com/reprints>.

**Correspondence and requests for materials** should be addressed to M.P. **Publisher's note:** Springer Nature remains neutral with regard to jurisdictional claims in published maps and institutional affiliations.

## METHODS

**Microscopic parameters.** The dynamics of the spinor Bose gas is described by the Hamiltonian

$$\hat{H} = \hat{H}_0 + \int dV \left[ \frac{c_0}{2} \hat{n}^2 + \frac{c_1}{2} (\hat{F}_x^2 + \hat{F}_y^2 + \hat{F}_z^2) : + q(\hat{n}_{+1} + \hat{n}_{-1}) + p\hat{F}_z \right] \quad (3)$$

where  $\hat{n}_m = \hat{\psi}_m^\dagger \hat{\psi}_m$ , with  $\hat{\psi}_m^\dagger$  the bosonic field creation operator of the magnetic substate  $m \in \{0, \pm 1\}$ , and  $:$  denotes normal ordering.  $\hat{H}_0$  contains the spin-independent kinetic energy and trapping potential. The spin operators are given by  $\hat{F}_x = [\hat{\psi}_0^\dagger(\hat{\psi}_{+1} + \hat{\psi}_{-1}) + \text{h.c.}]/\sqrt{2}$  and  $\hat{F}_y = [i\hat{\psi}_0^\dagger(\hat{\psi}_{+1} - \hat{\psi}_{-1}) + \text{h.c.}]/\sqrt{2}$  and  $\hat{F}_z = \hat{n}_{+1} - \hat{n}_{-1}$ . The parameter  $p$  describes the linear Zeeman shift in a magnetic field. For the hyperfine spin  $F=1$  of  $^{87}\text{Rb}$  the spin interaction is ferromagnetic, that is,  $c_1 < 0$ .

For the experimental control parameter  $q > 2n|c_1|$ , with  $n$  being the total density, the mean-field ground state is the polar state, which corresponds to all atoms occupying the  $m_F=0$  state. In the range  $0 < q < 2n|c_1|$  a spin with non-vanishing length in the  $x$ - $y$  plane is energetically favoured (easy-plane ferromagnet)<sup>32</sup>. This is the parameter regime employed in the experiment.

**Experimental system.** We prepare a Bose–Einstein condensate of about 70,000 atoms in the state  $(F, m_F) = (1, 0)$  in an optical dipole trap of 1,030 nm light with trapping frequencies  $\omega_{\parallel} \approx 2\pi \times 2.2$  Hz and  $\omega_{\perp} \approx 2\pi \times 250$  Hz.

The control parameter  $q$  is given by  $q = q_B - q_{MW}$ , where  $q_B \approx 2\pi \times 56$  Hz is the second-order Zeeman splitting in a magnetic field of  $B \approx 0.884$  G and  $q_{MW} = \Omega^2/4\delta$  is the energy shift due to the microwave dressing. For dressing<sup>33</sup> we use a power-stabilized microwave generator with resonant Rabi frequency  $\Omega \approx 2\pi \times 5.3$  kHz and  $\delta \approx 2\pi \times 137$  kHz blue detuned with respect to the  $(1, 0) \leftrightarrow (2, 0)$  transition. For the spin dynamics we adjust  $\Omega$  and  $\delta$  so that  $q \approx n|c_1|$  (with  $n|c_1| \approx -2\pi \times 2$  Hz). To monitor the long-term stability of  $q$  we do a reference measurement every 4 h (corresponding to about 250 experimental realizations). For this we observe spin dynamics for a fixed evolution time of 4 s as a function of the control parameter  $q$  (changing the detuning  $\delta$ ). Analysing the integrated side mode population we infer that the drifts of  $q$  are well below 0.5 Hz.

**Preparation of different initial conditions.** We prepare three initial conditions (see Fig. 4) that differ from the polar state. For initial condition 1 the control parameter is first set to  $q \approx n|c_1| + 1$  Hz. After 500 ms of spin dynamics at this value we quench to the final value  $q \approx n|c_1|$ . For the preparation of initial condition 2 we apply a resonant  $\pi/5$  radio-frequency pulse to populate the  $(1, \pm 1)$  states. After a hold time of 100 ms at a magnetic field gradient of around  $0.2 \mu\text{G} \mu\text{m}^{-1}$  in the longitudinal trap direction we apply a second  $\pi/5$  radio-frequency pulse. The combination of  $q$  and an inhomogeneous  $p$  during the hold time leads to a spatially modulated transversal spin on a length scale of  $\lambda \approx 80 \mu\text{m}$ . For initial condition 3

we populate homogeneously the  $(1, \pm 1)$  states with a short radio-frequency pulse such that  $(n_{+1} + n_{-1})/n \approx 0.1$ .

**Spin read-out.** The spin dynamics is initiated by quenching the control parameter. After a fixed evolution time  $t$  we apply a short magnetic field gradient pulse (Stern–Gerlach) in the  $z$ -direction and switch off the waveguide potential. Following a short time of flight (about 1 ms) we perform high-intensity absorption imaging with a resonant light pulse of duration 15  $\mu\text{s}$ . The resolution of the imaging system is about 1.2  $\mu\text{m}$ , corresponding to three pixels on the charge-coupled-device camera<sup>34</sup>; we accordingly bin the spin profiles by three pixels. As our Stern–Gerlach analysis is oriented in the  $z$ -direction, for the read-out of the spin in the  $x$ - $y$  plane we apply, before the magnetic field gradient, a radio-frequency pulse resonant with the transitions  $(1, 0) \leftrightarrow (1, \pm 1)$ .

The radio-frequency pulse can be modelled as a spin rotation described by the Hamiltonian  $\hat{H}_{\text{rf}} = \Omega_{\text{rf}} \hat{F}_y$  with resonant Rabi frequency  $\Omega_{\text{rf}} \approx 2\pi \times 17.5$  kHz. Applying a  $\pi/2$ -pulse of duration 14.3  $\mu\text{s}$ , the observable  $\hat{F}_x$  is mapped to the measurable density difference  $n_{+1} - n_{-1}$ .

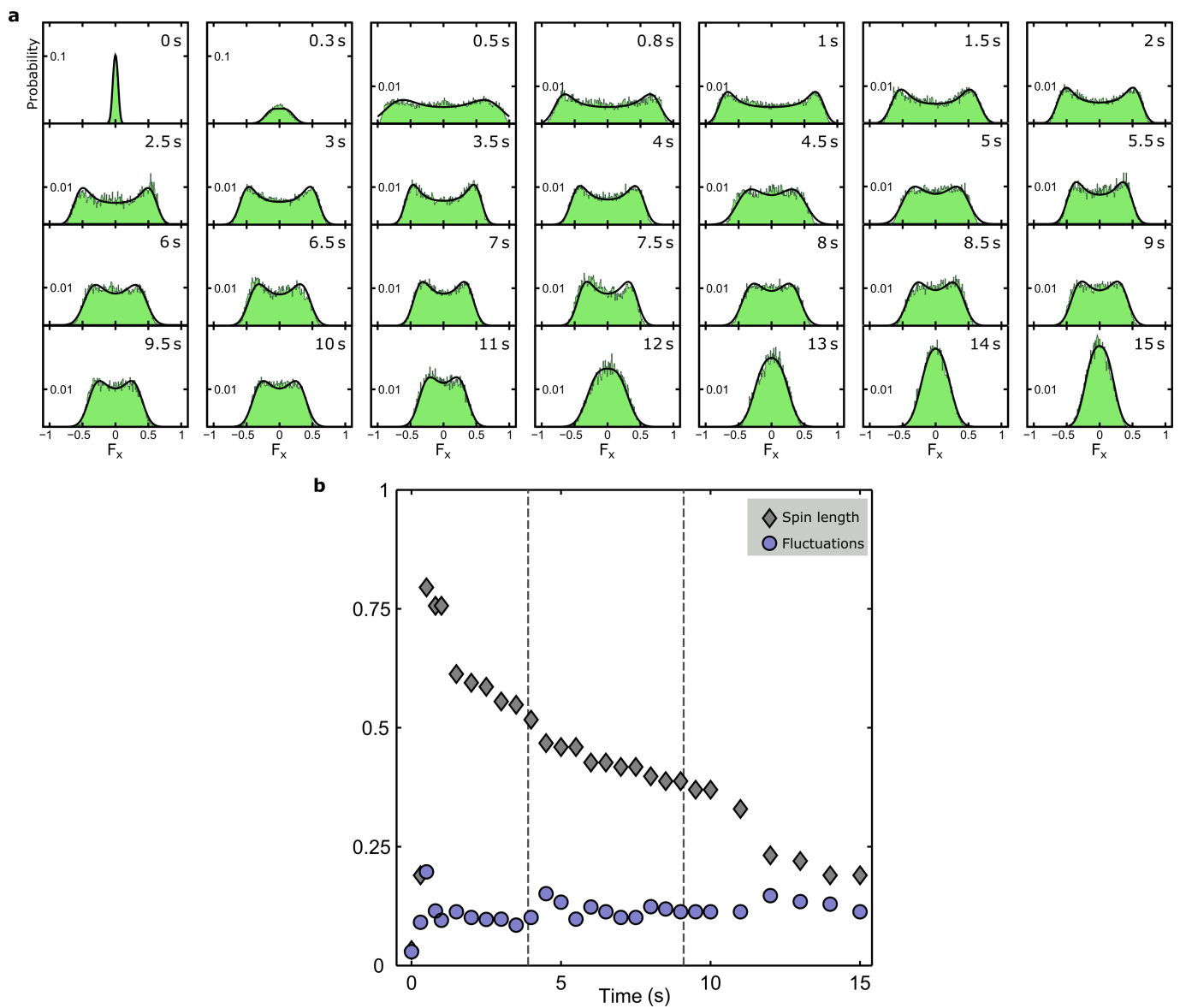
**Inferring the spin orientation.** The double-peaked spin distributions in the scaling regime (see Extended Data Fig. 1) resemble a distribution of a transversal spin with random orientation. To extract the corresponding ensemble average length  $\langle |F_{\perp}| \rangle$  of the transversal spin and its fluctuation  $\sigma$  we fit a probability density of the form  $p(F_x) \propto 1/\sqrt{1 - (F_x/\langle |F_{\perp}| \rangle)^2}$  convolved with a Gaussian distribution with root-mean-square  $\sigma$ . Under the assumption of a homogeneous spin length the spatial profile of the angular orientation is given by  $\theta(y) = \arcsin(F_x(y)/\langle |F_{\perp}| \rangle)$ . If the maximal amplitude is larger than  $\langle |F_{\perp}| \rangle - \sigma$  we use the maximal amplitude of the single realization instead of  $\langle |F_{\perp}| \rangle$ .

**Extraction of scaling exponents.** After rescaling the results of the discrete Fourier transform according to equation (2) we interpolate with cubic splines to obtain a common  $k$ -grid for all evolution times. We vary the scaling exponents  $\alpha$  and  $\beta$  to minimize the sum of the squared relative differences of all structure factors  $f_k$ . To estimate the statistical error on the exponents we employ a jackknife resampling analysis<sup>35</sup>.

## Data availability

The data presented in this paper are available from the corresponding author upon reasonable request.

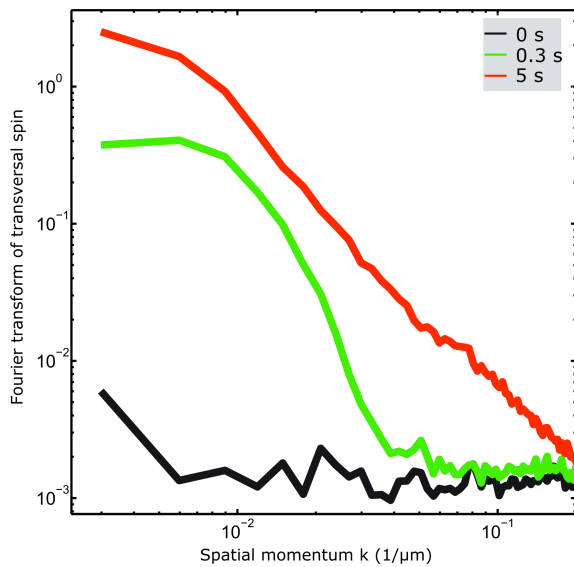
32. Kawaguchi, Y. & Ueda, M. Spinor Bose–Einstein condensates. *Phys. Rep.* **520**, 253–381 (2012).
33. Gerbier, F., Widera, A., Fölling, S., Mandel, O. & Bloch, I. Resonant control of spin dynamics in ultracold quantum gases by microwave dressing. *Phys. Rev. A* **73**, 041602(R) (2006).
34. Muessel, W. et al. Optimized absorption imaging of mesoscopic atomic clouds. *Appl. Phys. B* **113**, 69–73 (2013).
35. Miller, R. G. The jackknife—a review. *Biometrika* **61**, 1–15 (1974).



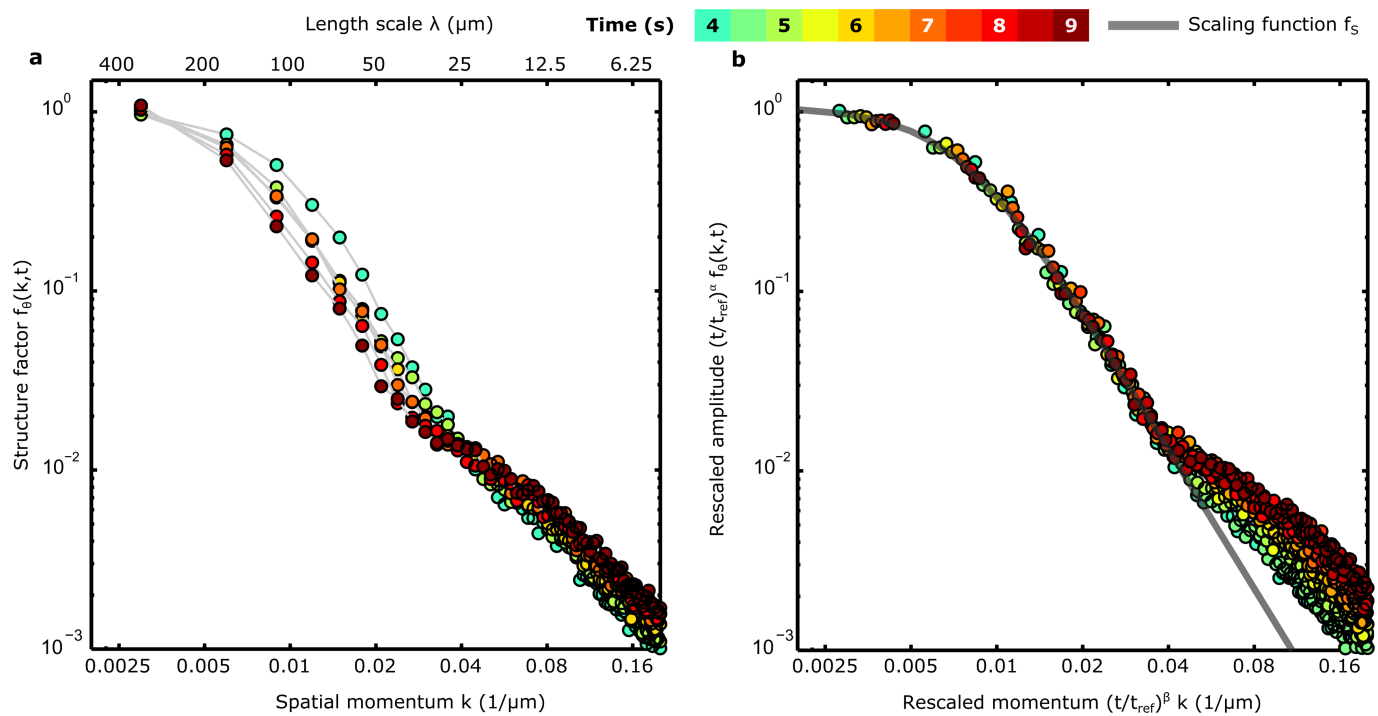
### Extended Data Fig. 1 | Spin distributions for all evolution times.

**a**, The panels show the distributions of the transversal spin,  $F_x$ , measured at different evolution times as indicated. Initially, we find a narrow Gaussian distribution corresponding to the prepared coherent spin state. The excitations developing in the transversal spin lead to a double-peaked distribution within the interval of 2 s to 10 s. For long evolution times,

$t > 12$  s, the distribution resembles a Gaussian, which is much broader than the initial distribution. **b**, The spin length and its root-mean-square fluctuation as a function of evolution time are extracted by a fit (see Methods). We find a slow decay of the spin length and nearly constant root-mean-square fluctuations in the scaling regime.



**Extended Data Fig. 2 | Build-up of transversal spin in momentum space.** Since the angular orientation  $\theta$  cannot be extracted reliably for short evolution times, we choose to show the Fourier transform of the transversal spin for regimes 1–3 (see Fig. 1). The initial condition, all atoms prepared in  $m_F=0$ , is characterized by a flat distribution. There is a fast build-up of long-wavelength spin excitations by more than two orders of magnitude within the first second. This process is followed by a redistribution of momenta leading to the scaling form for times longer than 4 s.



**Extended Data Fig. 3 | Scaling of structure factor for all experimentally accessible length scales.** Same data as shown in Fig. 2. **a**, Unscaled data. **b**, Data rescaled with the scaling exponents reported in the main text. The rescaling does not apply for large momenta,  $k > 0.04 \mu\text{m}^{-1}$ .